Preprint
UCRL-JC-142907

The Moment Condensed History Algorithm for Monte Carlo Electron Transport Simulations

D. R. Tolar, Jr., E. W. Larsen

This article was submitted to
2001 American Nuclear Society International Meeting on
Mathematical Methods for Nuclear Applications, Salt Lake City, UT,
September 9-13, 2001

February 27, 2001

U.S. Department of Energy
Lawrence Livermore National Laboratory

This work was performed under the auspices of the United States Department of Energy by the University of California, Lawrence Livermore National Laboratory under contract No. W-7405-Eng-48.

THE MOMENT CONDENSED HISTORY ALGORITHM FOR MONTE CARLO ELECTRON TRANSPORT SIMULATIONS

Danny R. Tolar, Jr.
Defense and Nuclear Technologies
Lawrence Livermore National Laboratory
Livermore, California 94551 USA
tolar1@llnl.gov

Edward W. Larsen
Department of Nuclear Engineering and Radiological Sciences
University of Michigan
Ann Arbor, Michigan 48109 USA
edlarsen@umich.edu

Keywords: electron transport, Monte Carlo, method of moments

ABSTRACT

We introduce a new Condensed History algorithm for the Monte Carlo simulation of electron transport. To obtain more accurate simulations, the new algorithm preserves the mean position and the variance in the mean position exactly for electrons that have traveled a given path length *and* are traveling in a given direction. This is accomplished by deriving the zeroth-, first-, and second-order *spatial* moments of the Spencer-Lewis equation and employing this information directly in the Condensed History process. Numerical calculations demonstrate the advantages of our method over standard Condensed History methods.

1. INTRODUCTION

Monte Carlo Condensed History (CH) algorithms are often used to simulate electron transport processes. These methods overcome the computational burdens of single collision models by "condensing" multiple electron collisions into large *steps* of user-specified path length s_0. Each Monte Carlo electron travels this path length in each CH step. Existing CH schemes employ a splitting routine (Larsen, 1992) over the range $0 < s < s_0$ to approximate the Boltzmann transport process. Berger (1965) devised a method in which the path length step is split into two substeps, each with size $s_0/2$. A more accurate "Random Hinge" CH method (Baro, 1995) splits the step into two substeps "randomly;" the first substep has length ξs_0, while the second has size $(1-\xi)s_0$, with ξ a random number on the unit interval.

These conventional CH algorithms are effective for many problems (Ballinger, 1992). However, they become inaccurate when the scattering becomes less forward-peaked. This occurs particularly at low energies (E < 100 keV) or in heavy (Z > 40) materials. In this case, conventional CH methods often fail to determine the electron's position accurately.

In this paper we describe a new non-splitting CH algorithm that more accurately determines the particles' locations. This is accomplished by preserving the mean position of electrons as well as the variances in the mean position. These means and variances are obtained directly from the zeroth-, first-, and second-order *spatial* moments of the Boltzmann equation. Thus, our new algorithm is related to the "Method of Moments," in which space-angle moments of ψ are obtained exactly (Shultis, 1996). [Our CH algorithm requires only spatial moments.]

The Method of Moments has been used to model many radiation transport problems. For electrons, a "moment" analysis has been performed by Larsen (1997) for pencil beam problems to obtain analytic expressions for the dose. While this effort is somewhat related to the research presented in this paper, Lewis' (1950) moment analysis for multiple scattering is more relevant. Lewis has derived the zeroth-, first-, and second-order *space-angle* moments of the Spencer-Lewis equation. Thus, he obtains quantities such as the mean depth for all particles that have traveled a path length s, regardless of the direction of flight at the end of the step. Our research is an extension of Lewis' work; the moments that we derive are spatial moments only – which are functions of both s *and* direction $\underline{\Omega}$. Thus, we obtain quantities such as the mean depth for all particles that, upon traveling a path length s, are traveling in a specified direction $\underline{\Omega}$. [This extra information is required for a Monte Carlo simulation.] When our moments are integrated over all $\underline{\Omega}$, Lewis' moments are obtained. Also, we incorporate these new moments, which are defined by infinite series and are more costly to evaluate than the Lewis moments, into a Monte Carlo Condensed History algorithm.

In Section 2, we derive the equations for the spatial moments, and their solutions. In Section 3, we describe how these solutions yield quantities such as the Goudsmit-Saunderson distribution, the mean position, and the variances in the mean position. In Section 4, we describe a new *Moment Condensed History* (MCH) algorithm, which preserves these moments. In Section 5, we compare numerical results using MCH with results from standard Condensed History schemes. These numerical results, which include energy deposition (dose) calculations, illustrate the power of the MCH method. We conclude with a brief summary in Section 6.

2. SPATIAL-MOMENT DERIVATIONS

We begin with the Spencer-Lewis equation, which is derived from the Boltzmann transport equation by applying the Continuous Slowing Down (CSD) approximation (Tolar, 1999). In the CSD approximation, particles lose energy continuously as they travel in a medium. Thus, through the stopping power, an electron's energy is directly related to the path length s. The Spencer-Lewis equation is given as

$$\frac{\partial}{\partial s}\psi\left(\underline{r},\underline{\Omega},s\right) + \underline{\Omega}\cdot\underline{\nabla}\psi\left(\underline{r},\underline{\Omega},s\right) + \Sigma_s\,\psi\left(\underline{r},\underline{\Omega},s\right) = \int \Sigma_s(\underline{\Omega}\cdot\underline{\Omega}')\,\psi(\underline{r},\underline{\Omega}',s)\,d\Omega' \ , \quad (1)$$

where

$$\underline{r} = (x,y,z) = \text{spatial variable} \ , \quad (2)$$

$$\underline{\Omega} = (\Omega_x,\Omega_y,\Omega_z) = (\sqrt{1-\mu^2}\cos\phi, \sqrt{1-\mu^2}\sin\phi, \mu) = \text{angular variable} \ , \quad (3)$$

$$\Sigma_s = \Sigma_{s0} = \text{macroscopic scattering cross section} \ , \quad (4)$$

and

$$\Sigma_s(\underline{\Omega}\cdot\underline{\Omega}') = \frac{1}{2\pi}\sum_{m=-\infty}^{\infty} e^{i\,m(\phi-\phi')}\,\Sigma_{sm}(\mu,\mu') \ , \quad (5)$$

with

$$\Sigma_{sm}(\mu,\mu') = \sum_{n=|m|}^{\infty} \left(\frac{2n+1}{2}\right) \frac{(n-|m|)!}{(n+|m|)!} \Sigma_{sn}\, P_{n,m}(\mu)\, P_{n,m}(\mu') \quad . \tag{6}$$

Here $P_{n,m}(\mu)$ are the Associated Legendre functions. The Legendre polynomials correspond to order $m = 0$: $P_n(\mu) = P_{n,0}(\mu)$. The initial condition specifies one particle at the origin of coordinates, traveling along the z-axis in the direction $\mu = 1$:

$$\psi(\underline{r}, \underline{\Omega}, 0) = \delta(x)\delta(y)\delta(z)\, \frac{\delta(\mu-1)}{2\pi} \quad . \tag{7}$$

The equations representing various spatial moments of $\psi(\underline{r}, \underline{\Omega}, s)$ are derived next.

2.1 Zeroth-Order Moment

To obtain the zeroth-order spatial moment, we integrate Eqs. (1) and (7) over all space. That is, we operate on these equations by $\int_{-\infty}^{\infty}(\cdot)\, d^3r$, and we define the following function:

$$\psi_0(\underline{\Omega}, s) \equiv \int_{-\infty}^{\infty} \psi\,(\underline{r}, \underline{\Omega}, s)\; d^3r \quad . \tag{8}$$

Upon performing this operation, the following equation for $\psi_0(\underline{\Omega}, s)$ is obtained:

$$\frac{\partial}{\partial s}\psi_0(\underline{\Omega}, s) + \Sigma_s \psi_0(\underline{\Omega}, s) = \int_{4\pi} \Sigma_s(\underline{\Omega}\cdot\underline{\Omega}')\, \psi_0(\underline{\Omega}', s)\, d\Omega' \quad , \tag{9}$$

with initial condition:

$$\psi_0(\underline{\Omega}, 0) = \frac{\delta(\mu-1)}{2\pi} \quad . \tag{10}$$

[Integrating the second (leakage) term in Eq. (1) over all space yields zero, since by assumption $\psi\,(\underline{r}, \underline{\Omega}, s)$ vanishes at $|\underline{r}| = \infty$.] For the initial condition given by Eq. (10), $\psi_0(\underline{\Omega}, s)$ in Eq. (9) can be solved analytically by expanding in Legendre polynomials. The solution is

$$\psi_0(\underline{\Omega}, s) = \psi_0(\mu, s) = \sum_{n=0}^{\infty} \frac{2n+1}{4\pi} P_n(\mu)\, \exp(-\Sigma_{an} s) \quad , \tag{11}$$

where $\Sigma_{an} = \Sigma_{s0} - \Sigma_{sn}$. $\psi_0(\mu, s)$ is the *Goudsmit-Saunderson* distribution (Goudsmit, 1940), the exact probability distribution for the direction of flight $\underline{\Omega}$ of particles that have traveled a path length s. By Eq. (11), the azimuthal scattering angle ϕ is sampled uniformly on $0 \le \phi < 2\pi$, while the cosine of the scattering angle is sampled from the distribution function $2\pi\psi_0(\mu, s)$ for μ.

2.2 First-Order Moments

In Cartesian geometry, three first-order spatial moments exist. One moment involves the *depth* coordinate z; the other two pertain to the *transverse* coordinates x and y.

To obtain the first-order moments, we operate on Eqs. (1) and (7) by $\int_{-\infty}^{\infty} x_i(\cdot)\, d^3r$, and define the functions $\psi_{x_i}(\underline{\Omega}, s)$ as

$$\psi_{x_i}(\underline{\Omega}, s) \equiv \int_{-\infty}^{\infty} x_i\, \psi\,(\underline{r}, \underline{\Omega}, s)\; d^3r \quad , \tag{12}$$

with

$$x_i = \begin{cases} x & : \quad i = 1 \\ y & : \quad i = 2 \\ z & : \quad i = 3 \end{cases} \quad .$$

After an integration by parts on the leakage term, the following differential equation and initial condition are obtained for $\psi_{x_i}(\underline{\Omega}, s)$:

$$\frac{\partial}{\partial s}\psi_{x_i}(\underline{\Omega}, s) + \Sigma_s\, \psi_{x_i}(\underline{\Omega}, s) - \int_{4\pi} \Sigma_s(\underline{\Omega} \cdot \underline{\Omega}')\, \psi_{x_i}(\underline{\Omega}', s)\, d\Omega' = \Omega_{x_i}\, \psi_0(\mu, s) \quad , \tag{13}$$

$$\psi_{x_i}(\underline{\Omega}, 0) = 0 \quad . \tag{14}$$

These problems contain, in the source terms, the (known) Goudsmit-Saunderson distribution function $\psi_0(\mu, s)$.

For the depth-coordinate z $(i = 3)$, the solution to Eqs. (13) and (14) can be solved analytically for $\psi_z(\underline{\Omega}, s)$ by expanding in Legendre polynomials. Omitting the algebraic details, the result is:

$$\begin{aligned} \psi_z(\underline{\Omega}, s) = \psi_z(\mu, s) \quad &= \quad \sum_{n=0}^{\infty} \frac{P_n(\mu)}{4\pi} \left\{ n \left[\frac{\exp(-\Sigma_{an} s) - \exp(-\Sigma_{a,n-1} s)}{\Sigma_{sn} - \Sigma_{s,n-1}} \right] \right. \\ &+ \quad \left. (n+1) \left[\frac{\exp(-\Sigma_{an} s) - \exp(-\Sigma_{a,n+1} s)}{\Sigma_{sn} - \Sigma_{s,n+1}} \right] \right\} \quad . \end{aligned} \tag{15}$$

For the transverse coordinates x $(i = 1)$ and y $(i = 2)$, the solutions $\psi_x(\underline{\Omega}, s)$ and $\psi_y(\underline{\Omega}, s)$ of Eqs. (13) and (14) can be obtained by expanding in Associated Legendre functions of order $m = 1$. Omitting the algebraic details, we obtain:

$$\psi_x(\underline{\Omega}, s) = \psi_1(\mu, s) \cos\phi \quad , \tag{16}$$

$$\psi_y(\underline{\Omega}, s) = \psi_1(\mu, s)\, \sin\phi \quad , \tag{17}$$

where

$$\begin{aligned} \psi_1(\mu, s) \quad &= \quad \sum_{n=1}^{\infty} \frac{P_{n,1}(\mu)}{4\pi} \left[\frac{\exp(-\Sigma_{a,n-1} s) - \exp(-\Sigma_{an} s)}{\Sigma_{s,n-1} - \Sigma_{sn}} \right. \\ &- \quad \left. \frac{\exp(-\Sigma_{a,n+1} s) - \exp(-\Sigma_{an} s)}{\Sigma_{s,n+1} - \Sigma_{sn}} \right] \quad . \end{aligned} \tag{18}$$

2.3 Second-Order Moments

Now we investigate the second-order spatial moments. Six of these moments exist: $z^2, x^2, y^2, xz = zx, yz = zy$, and $xy = yx$. Unfortunately, the solutions for these moments are algebraically complicated. Despite this complexity, we have shown (Tolar, 1999) that including the second-order moments is vital in creating a successful MCH algorithm.

Similar to Sections 2.1 and 2.2, we operate on Eqs. (1) and (7) by $\int_{-\infty}^{\infty} x_i\, x_j\, (\cdot)\, d^3r$ and define the functions

$$\psi_{x_i x_j}(\underline{\Omega}, s) \equiv \int_{-\infty}^{\infty} x_i\, x_j\, \psi\, (\underline{r}, \underline{\Omega}, s)\, d^3r \quad , \tag{19}$$

with

$$x_i x_j = \begin{cases} xx & : \quad i = j = 1 \\ yy & : \quad i = j = 2 \\ zz & : \quad i = j = 3 \\ xz & : \quad i = 1, j = 3 \\ yz & : \quad i = 2, j = 3 \\ xy & : \quad i = 1, j = 2 \end{cases} .$$

After an integration by parts on the leakage term, the following equation and initial condition are obtained for $\psi_{x_i x_j}(\underline{\Omega}, s)$:

$$\frac{\partial}{\partial s}\psi_{x_i x_j}(\underline{\Omega}, s) + \Sigma_s \, \psi_{x_i x_j}(\underline{\Omega}, s) - \int_{4\pi} \Sigma_s(\underline{\Omega} \cdot \underline{\Omega}')\psi_{x_i x_j}(\underline{\Omega}', s) \, d\Omega'$$

$$= \Omega_{x_j} \, \psi_{x_i}(\underline{\Omega}, s) + \Omega_{x_i} \, \psi_{x_j}(\underline{\Omega}, s) \quad , \tag{20}$$

$$\psi_{x_i x_j}(\underline{\Omega}, 0) = 0 \quad . \tag{21}$$

These equations contain, in their source terms, the (known) first-order moment functions described above. The solutions of Eqs. (20) and (21) can be derived by expanding in higher-order Associated Legendre functions. Omitting the lengthy algebraic details, we obtain the following results.

For $i = j = 3$,

$$\begin{aligned} \psi_{zz}(\underline{\Omega}, s) \;=\; & \sum_{n=0}^{\infty} \frac{P_n(\mu)}{2\pi} \left\{ \frac{n+1}{2n+3} \left[\frac{n+1}{\Sigma_{s,n+1} - \Sigma_{sn}} \left(\frac{\exp(-\Sigma_{a,n+1}s) - \exp(-\Sigma_{an}s)}{\Sigma_{s,n+1} - \Sigma_{sn}} \right.\right.\right. \\ & - \left. s \exp(-\Sigma_{an}s) \right) + \frac{n+2}{\Sigma_{s,n+1} - \Sigma_{s,n+2}} \left(\frac{\exp(-\Sigma_{a,n+1}s) - \exp(-\Sigma_{an}s)}{\Sigma_{s,n+1} - \Sigma_{sn}} \right. \\ & - \left. \left. \frac{\exp(-\Sigma_{a,n+2}s) - \exp(-\Sigma_{an}s)}{\Sigma_{s,n+2} - \Sigma_{sn}} \right) \right] + \frac{n}{2n-1} \left[\frac{n-1}{\Sigma_{s,n-1} - \Sigma_{s,n-2}} \right. \\ & \left(\frac{\exp(-\Sigma_{a,n-1}s) - \exp(-\Sigma_{an}s)}{\Sigma_{s,n-1} - \Sigma_{sn}} - \frac{\exp(-\Sigma_{a,n-2}s) - \exp(-\Sigma_{an}s)}{\Sigma_{s,n-2} - \Sigma_{sn}} \right) \\ & + \frac{n}{\Sigma_{s,n-1} - \Sigma_{sn}} \left(\frac{\exp(-\Sigma_{a,n-1}s) - \exp(-\Sigma_{an}s)}{\Sigma_{s,n-1} - \Sigma_{sn}} \right. \\ & \left. \left. \left. \left. - \, s \exp(-\Sigma_{an}s) \right) \right] \right\} = \psi_{zz}(\mu, s) \quad . \end{aligned} \tag{22}$$

For $i = j = 1$ and $i = j = 2$,

$$\psi_{xx}(\underline{\Omega}, s) = \psi_2^a(\mu, s) + \psi_2^b(\mu, s) \, \cos 2\phi \quad , \tag{23}$$

and

$$\psi_{yy}(\underline{\Omega}, s) = \psi_2^a(\mu, s) - \psi_2^b(\mu, s) \, \cos 2\phi \quad , \tag{24}$$

where

$$\psi_2^a(\mu,s) = \sum_{n=0}^{\infty}\frac{P_n(\mu)}{4\pi}\left\{\frac{(n+1)(n+2)}{2n+3}\left[\frac{1}{\Sigma_{sn}-\Sigma_{s,n+1}}\left(s\exp(-\Sigma_{an}s)\right.\right.\right.$$
$$\left.-\frac{\exp(-\Sigma_{a,n+1}s)-\exp(-\Sigma_{an}s)}{\Sigma_{s,n+1}-\Sigma_{sn}}\right)-\frac{1}{\Sigma_{s,n+2}-\Sigma_{s,n+1}}$$
$$\left.\left(\frac{\exp(-\Sigma_{a,n+2}s)-\exp(-\Sigma_{an}s)}{\Sigma_{s,n+2}-\Sigma_{sn}}-\frac{\exp(-\Sigma_{a,n+1}s)-\exp(-\Sigma_{an}s)}{\Sigma_{s,n+1}-\Sigma_{sn}}\right)\right]$$
$$-\frac{n(n-1)}{2n-1}\left[\frac{1}{\Sigma_{s,n-2}-\Sigma_{s,n-1}}\left(\frac{\exp(-\Sigma_{a,n-2}s)-\exp(-\Sigma_{an}s)}{\Sigma_{s,n-2}-\Sigma_{sn}}\right.\right.$$
$$\left.-\frac{\exp(-\Sigma_{a,n-1}s)-\exp(-\Sigma_{an}s)}{\Sigma_{s,n-1}-\Sigma_{sn}}\right)-\frac{1}{\Sigma_{sn}-\Sigma_{s,n-1}}$$
$$\left.\left.\left(s\exp(-\Sigma_{an}s)-\frac{\exp(-\Sigma_{a,n-1}s)-\exp(-\Sigma_{an}s)}{\Sigma_{s,n-1}-\Sigma_{sn}}\right)\right]\right\}\ , \tag{25}$$

and

$$\psi_2^b(\mu,s) = \sum_{n=2}^{\infty}\frac{P_{n,2}(\mu)}{4\pi}\left\{\frac{1}{2n-1}\left[\frac{1}{\Sigma_{s,n-2}-\Sigma_{s,n-1}}\left(\frac{\exp(-\Sigma_{a,n-2}s)-\exp(-\Sigma_{an}s)}{\Sigma_{s,n-2}-\Sigma_{sn}}\right.\right.\right.$$
$$\left.-\frac{\exp(-\Sigma_{a,n-1}s)-\exp(-\Sigma_{an}s)}{\Sigma_{s,n-1}-\Sigma_{sn}}\right)-\frac{1}{\Sigma_{sn}-\Sigma_{s,n-1}}\left(s\exp(-\Sigma_{an}s)\right.$$
$$\left.\left.-\frac{\exp(-\Sigma_{a,n-1}s)-\exp(-\Sigma_{an}s)}{\Sigma_{s,n-1}-\Sigma_{sn}}\right)\right]-\frac{1}{2n+3}\left[\frac{1}{\Sigma_{sn}-\Sigma_{s,n+1}}\right.$$
$$\left.\left(s\exp(-\Sigma_{an}s)-\frac{\exp(-\Sigma_{a,n+1}s)-\exp(-\Sigma_{an}s)}{\Sigma_{s,n+1}-\Sigma_{sn}}\right)\right.$$
$$-\frac{1}{\Sigma_{s,n+2}-\Sigma_{s,n+1}}\left(\frac{\exp(-\Sigma_{a,n+2}s)-\exp(-\Sigma_{an}s)}{\Sigma_{s,n+2}-\Sigma_{sn}}\right.$$
$$\left.\left.\left.-\frac{\exp(-\Sigma_{a,n+1}s)-\exp(-\Sigma_{an}s)}{\Sigma_{s,n+1}-\Sigma_{sn}}\right)\right]\right\}\ . \tag{26}$$

For $i=1, j=2$,

$$\psi_{xy}(\underline{\Omega},s) = \psi_2^b(\mu,s)\,\sin 2\phi\ . \tag{27}$$

Finally, for $i=1, j=3$ and $i=2, j=3$,

$$\psi_{xz}(\underline{\Omega},s) = \psi_3(\mu,s)\,\cos\phi\ , \tag{28}$$

and

$$\psi_{yz}(\underline{\Omega},s) = \psi_3(\mu,s)\,\sin\phi\ , \tag{29}$$

where

$$
\begin{aligned}
\psi_3(\mu, s) \;=\; & \sum_{n=1}^{\infty} \frac{P_{n,1}(\mu)}{4\pi} \Bigg\{ \frac{1}{2n-1} \Bigg[\frac{2(n-1)}{\Sigma_{s,n-1} - \Sigma_{s,n-2}} \Bigg(\frac{\exp(-\Sigma_{a,n-1}s) - \exp(-\Sigma_{an}s)}{\Sigma_{s,n-1} - \Sigma_{sn}} \\
& - \frac{\exp(-\Sigma_{a,n-2}s) - \exp(-\Sigma_{an}s)}{\Sigma_{s,n-2} - \Sigma_{sn}} \Bigg) + \frac{1}{\Sigma_{sn} - \Sigma_{s,n-1}} \\
& \left(s \exp(-\Sigma_{an}s) - \frac{\exp(-\Sigma_{a,n-1}s) - \exp(-\Sigma_{an}s)}{\Sigma_{s,n-1} - \Sigma_{sn}} \right) \Bigg] \\
& - \frac{1}{2n+3} \Bigg[\frac{2(n+2)}{\Sigma_{s,n+1} - \Sigma_{s,n+2}} \Bigg(\frac{\exp(-\Sigma_{a,n+1}s) - \exp(-\Sigma_{an}s)}{\Sigma_{s,n+1} - \Sigma_{sn}} \\
& - \frac{\exp(-\Sigma_{a,n+2}s) - \exp(-\Sigma_{an}s)}{\Sigma_{s,n+2} - \Sigma_{sn}} \Bigg) - \frac{1}{\Sigma_{sn} - \Sigma_{s,n+1}} \Bigg(s \exp(-\Sigma_{an}s) \\
& - \frac{\exp(-\Sigma_{a,n+1}s) - \exp(-\Sigma_{an}s)}{\Sigma_{s,n+1} - \Sigma_{sn}} \Bigg) \Bigg] \Bigg\} \; . \qquad (30)
\end{aligned}
$$

3. UTILIZING THE SPATIAL MOMENTS

We now describe how to utilize the spatial moments of the Spencer-Lewis equation. The zeroth-order moment provides the Goudsmit-Saunderson distribution. The zeroth- and first-order moments provide the mean or average coordinates, $(\langle x \rangle, \langle y \rangle, \langle z \rangle)$, each of which are functions of $\underline{\Omega}$ and s. The zeroth- and second-order moments enable the variances in the mean coordinates, $(\sigma_x^2, \sigma_y^2, \sigma_z^2)$, to be determined, as well as the co-variances: $(\sigma_{xy}^2, \sigma_{xz}^2, \sigma_{yz}^2)$; each of these six quantities are also functions of $\underline{\Omega}$ and s. In the following subsections, we discuss these quantities.

3.1 The Goudsmit-Saunderson Distribution

The zeroth-order spatial moment, $\psi_0(\underline{\Omega}, s)$, is the Goudsmit-Saunderson distribution. As stated in Section 2.1, ψ_0 is the probability distribution function for $\underline{\Omega}$ for particles that have traveled a path length s. Thus, in every Condensed History step, the direction of flight $\underline{\Omega}$ is sampled from $\psi_0(\underline{\Omega}, s)$. Doing this is standard practice in conventional CH methods, and we retain this in the MCH method.

3.2 The Mean Coordinates

Now, we determine the mean position for electrons that, after traveling a path length s (specified by the user), are traveling the the direction $\underline{\Omega}$ (obtained from the Goudsmit-Saunderson distribution). These mean positions are preserved in our new algorithm, but not in conventional Condensed History methods.

We define the function $\langle x_i \rangle(\underline{\Omega}, s)$ as

$$
\langle x_i \rangle(\underline{\Omega}, s) \equiv \frac{\int_{-\infty}^{\infty} x_i \, \psi(\underline{r}, \underline{\Omega}, s) \, d^3r}{\int_{-\infty}^{\infty} \psi(\underline{r}, \underline{\Omega}, s) \, d^3r} \; . \qquad (31)
$$

For $x_3 = z$ $(i = 3)$, $\langle z \rangle(\underline{\Omega}, s)$ is the mean z-coordinate or *depth* of particles that, upon traveling a path length s, are traveling in the direction $\underline{\Omega}$. From Eqs. (12) and (8),

$\langle z \rangle$ can be written as

$$\langle z \rangle(\underline{\Omega}, s) = \langle z \rangle(\mu, s) = \frac{\psi_z(\mu, s)}{\psi_0(\mu, s)} \quad . \tag{32}$$

Before proceeding, we state an interesting result. The mean value of z for $\mu = -1$ is zero for *all* $s > 0$. By setting $\mu = -1$ in Eq. (15), we see the expression for $\psi_z(-1, s)$ on the right side is zero. This result holds for any differential scattering cross section—it is a universal result.

Likewise, the mean values of x and y of particles that, upon traveling a path length s, are traveling in the direction $\underline{\Omega}$, are

$$\langle x \rangle(\underline{\Omega}, s) = \frac{\psi_1(\mu, s)}{\psi_0(\mu, s)} \cos\phi \quad , \tag{33}$$

and

$$\langle y \rangle(\underline{\Omega}, s) = \frac{\psi_1(\mu, s)}{\psi_0(\mu, s)} \sin\phi \quad . \tag{34}$$

3.3 The Variances in the Mean Coordinates

The second-order spatial moments obtained in Section 2.3 allow the variances in the mean coordinates (as well as all the co-variances) to be determined. Before proceeding, it is useful to develop a general definition of the variance between two coordinates $x_i x_j$. (The standard deviation $\sigma_{x_i x_j}(\underline{\Omega}, s)$ is the square root of the variance.) This variance is a function of both $\underline{\Omega}$ and s, defined by

$$\sigma^2_{x_i x_j}(\underline{\Omega}, s) \equiv \frac{\int_{-\infty}^{\infty} (x_i - \langle x_i \rangle)\,(x_j - \langle x_j \rangle)\,\psi\,(\underline{r}, \underline{\Omega}, s)\; d^3r}{\int_{-\infty}^{\infty} \psi\,(\underline{r}, \underline{\Omega}, s)\; d^3r} \quad . \tag{35}$$

Multiplying the two terms in parenthesis and expanding, we obtain:

$$\sigma^2_{x_i x_j}(\underline{\Omega}, s) = \langle x_i x_j \rangle(\underline{\Omega}, s) - \langle x_i \rangle(\underline{\Omega}, s)\,\langle x_j \rangle(\underline{\Omega}, s) \quad , \tag{36}$$

where

$$\langle x_i x_j \rangle(\underline{\Omega}, s) \equiv \frac{\int_{-\infty}^{\infty} x_i x_j\,\psi\,(\underline{r}, \underline{\Omega}, s)\; d^3r}{\int_{-\infty}^{\infty} \psi\,(\underline{r}, \underline{\Omega}, s)\; d^3r} \quad ,$$

and $\langle x_i \rangle(\underline{\Omega}, s)$ is given by Eq. (31).

Thus, the three variances $\sigma^2_x(\underline{\Omega}, s)$, $\sigma^2_y(\underline{\Omega}, s)$, and $\sigma^2_z(\underline{\Omega}, s)$ are found for the cases $i = j$ using Eqs. (19), (12), and (8):

$$\sigma^2_{x_i x_i}(\underline{\Omega}, s) = \langle x_i^2 \rangle(\underline{\Omega}, s) - \langle x_i \rangle^2(\underline{\Omega}, s) \quad . \tag{37}$$

The three co-variances ($\sigma^2_{xy}(\underline{\Omega}, s)$, $\sigma^2_{xz}(\underline{\Omega}, s)$, and $\sigma^2_{yz}(\underline{\Omega}, s)$) are given by Eq. (36). These quantities are not zero because individual electrons only approximately travel to their mean location.

4. THE MOMENT CONDENSED HISTORY ALGORITHM

Now we describe the Monte Carlo MCH algorithm, which preserves the zeroth-, first-, and second-order spatial moments of the Spencer-Lewis equation. Each Condensed History step begins with the user prescribing the path length s, as well as the cross sections and stopping powers. Using the CSD approximation, the choice of s automatically determines the electron's energy at the end of the step.

Given s, the MCH algorithm samples $\underline{\Omega}$, the direction of flight at the end of the step, from the Goudsmit-Saunderson distribution. [This calculation happens in all CH methods.]

Next, with s and $\underline{\Omega}$ known, the mean position

$$\langle \underline{r} \rangle (\underline{\Omega}, s) = (\langle x \rangle (\underline{\Omega}, s), \langle y \rangle (\underline{\Omega}, s), \langle z \rangle (\underline{\Omega}, s))$$

is evaluated, and the Monte Carlo particle is temporarily placed there. In this step, MCH preserves the zeroth- and first-order spatial moments.

However, instead of rigidly forcing the Monte Carlo particle to remain at this (mean) location at the end of the step, a new position is determined by sampling spatial probability distribution functions *about* the mean position. These new distributions have zero means, and variances that are directly related to the variances and co-variances derived in Section 3.3. This zero-mean deviation from the mean location enables the second-order spatial moments to be preserved.

As long as they have the correct means and variances, any probability distribution function can be used to preserve the second-order moments. If we ever desire to preserve even higher-order moments, then the choice of these distribution functions must be made more carefully. To make the algorithm efficient, we would like to sample three independent, one-dimensional functions. For simplicity, we choose Gaussian distributions.

Unfortunately, in the (x, y, z) coordinate system, the particle's new position cannot be determined efficiently. This is a consequence of the non-zero co-variances: σ^2_{xy}, σ^2_{xz}, and σ^2_{yz}. However, a special coordinate system exists in which all co-variances *are* zero; thus, three independent one-dimensional Gaussians can be sampled to obtain the final position coordinates. These positions must be transformed back to (x, y, z) system. This transformation is determined by Tolar (1999) by diagonalizing the variance matrix. With the electron's energy, direction of flight, and (final) position known, a MCH step is complete, and one can proceed with subsequent steps in the same manner.

5. NUMERICAL COMPARISONS

We now compare MCH with Random Hinge and with analog Monte Carlo, using numerical results from simulations of two simple electron transport problems. Both problems involve initially monoenergetic pencil beams. As the electrons in the beam slow down to various energies, the mean position and the standard deviation in the mean are determined. In addition, we calculate the dose (energy deposited to the medium per unit mass) as a function of depth (z-coordinate).

We consider pencil beams of 20 MeV and 12.5 keV at the origin of the (x, y, z) coordinate system traveling down the z-axis in the direction $\mu = 1$. The beam is contained within an infinite, homogeneous medium of aluminum. Since aluminum has

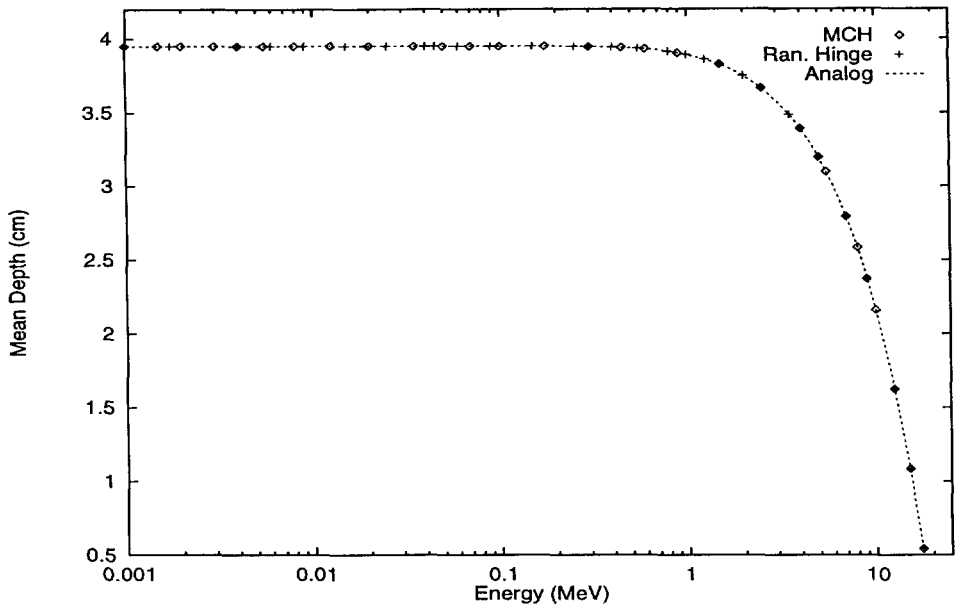

Figure 1: Mean Depth of Beam in Aluminum as a Function of Energy (E_0 = 20 MeV).

a low atomic number (Z=13), electrons with energies in the MeV range undergo highly forward-peaked scattering. However, as they lose energy, their scattering becomes more isotropic. In the 10 keV range, electrons in aluminum scatter fairly isotropically. Thus, these two problems provide two different conditions for testing the MCH and Random Hinge techniques.

All the simulations, (analog Monte Carlo, MCH, and Random Hinge) employ the CSD approximation. We also use the multigroup approximation to describe the energy dependence of the cross sections and stopping powers. For the Condensed History schemes, we select the step size s to be the path length required for an electron to lose the energy corresponding to the width of one energy group.

Problem 1: 20 MeV Electron Beam

The first three figures in this section present the results from a 20 MeV electron pencil beam problem. Figure 1 is a plot of the mean depth as a function of the electron beam energy. First, the analog Monte Carlo results are shown by a dashed line, and they match the exact solution given by Lewis (1950). Second, the results for the Random Hinge simulation are displayed by cross symbols (+). These calculations are virtually identical to analog Monte Carlo. Random Hinge's excellent accuracy is expected because high energy (MeV) electrons in aluminum undergo highly forward-peaked scattering. This forces nearly all electrons to stream down the z-axis with minimal transverse deflection until they have reached energies around 10 keV. Conventional Condensed History algorithms like Random Hinge are effective under these conditions. Third, the MCH results, depicted by diamond symbols ($\diamond$), also reproduce the analog Monte Carlo results. This is because $\langle z \rangle(E)$ is automatically preserved in this algorithm.

The standard deviation in the mean depth (denoted by sig_z) and the rms radius (denoted by sig_r) are shown in Figure 2 as functions of energy. Similar to

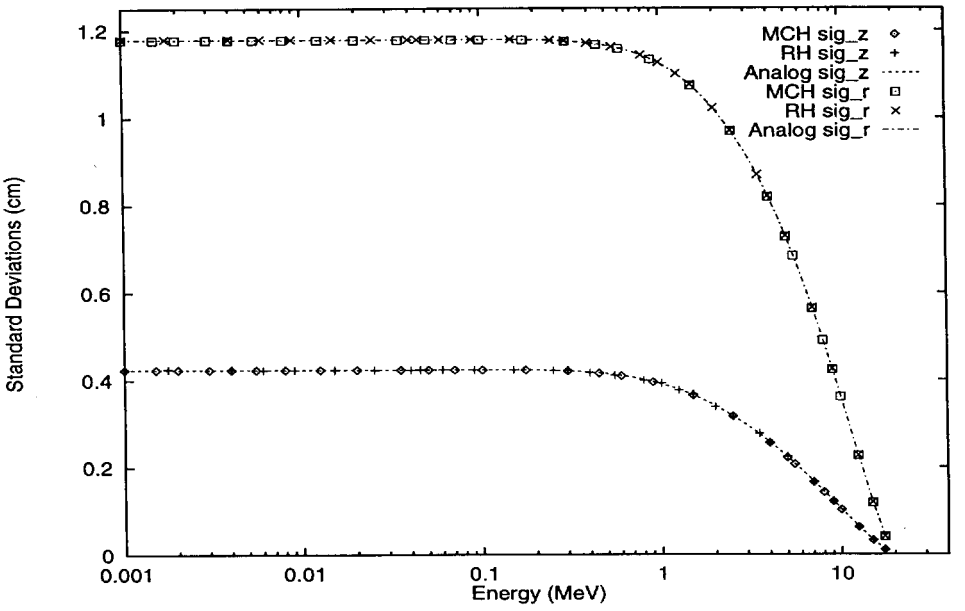

Figure 2: Standard Deviation in Mean Depth (sig_z) and RMS Radius (sig_r) of Beam in Aluminum as a Function of Energy ($E_0 = 20$ MeV).

Figure 1, the results from all the simulations compare very closely to one another. MCH reproduces these second-order quantities automatically. All simulations match the exact moments derived by Lewis (1950).

Figure 3 displays the dose as a function of depth. For this problem, an analytical solution cannot be obtained. Furthermore, unlike the previous calculations, the dose is not preserved in the MCH algorithm. Nevertheless, Figure 3 indicates very precise agreement between all three methods. (The three lines lie on top of one another.) The plot also indicates that nearly zero dose is delivered to any depth to the left of the origin; that is, very few particles with MeV energies backscatter in aluminum.

Problem 2: 12.5 keV Electron Beam

The next three figures are plots of the same parameters for a 12.5 keV electron pencil beam in aluminum. Here we see a disparity between the Random Hinge and analog Monte Carlo results. Because electrons in this energy range undergo weakly anisotropic scattering, Random Hinge cannot accurately predict the mean depth or the standard deviations. In Figure 4, Random Hinge estimates a mean depth that is about 4.5% higher than the exact solution (analog Monte Carlo). In fact, Kawrakow and Bielajew (1998) have shown that Random Hinge is no more accurate than Berger's second method in determining $\langle z \rangle(E)$. MCH, on the other hand, reproduces the mean depth exactly. Again, this is an intrinsic feature of the MCH algorithm, which is independent of the electrons' energies or how they scatter.

It should be mentioned that the spatial dimensions for the 12.5 keV problem are about five orders of magnitude smaller than the dimensions for the 20 MeV problem. This is because electrons travel much shorter path lengths in slowing down from 12.5 keV than electrons that slow down from 20 MeV. Furthermore, 12.5 keV electrons undergo substantial transverse displacement at much smaller depths than

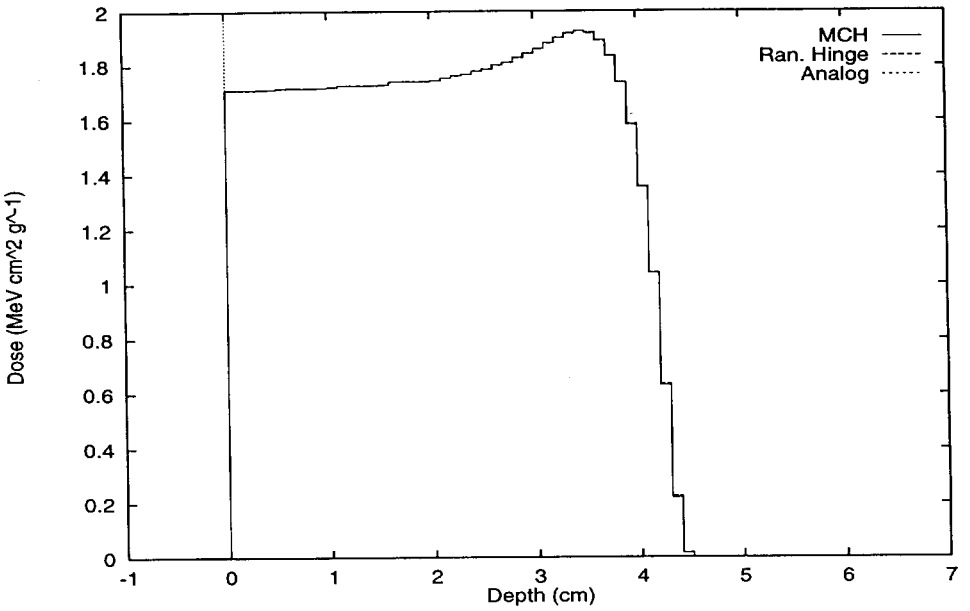

Figure 3: Dose Deposited as a Function of Depth into Aluminum ($E_0 = 20$ MeV).

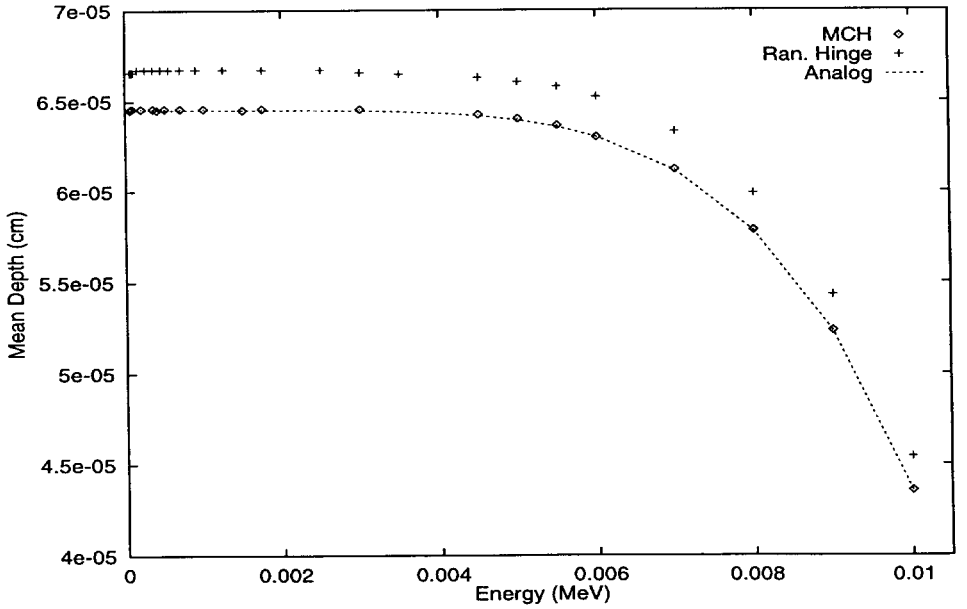

Figure 4: Mean Depth of Electron Beam in Aluminum as a Function of Energy ($E_0 = 12.5$ keV).

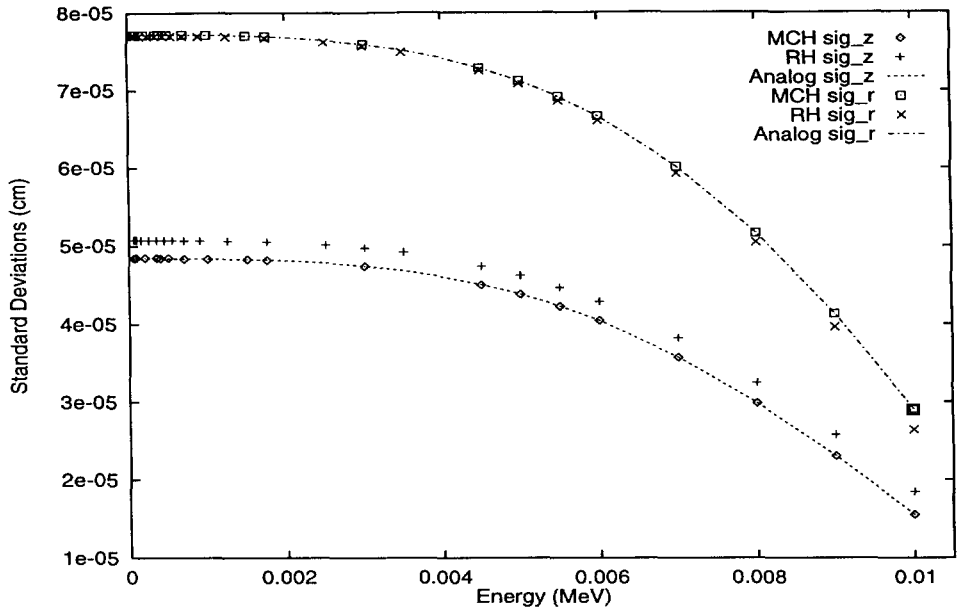

Figure 5: Standard Deviation in Mean Depth (sig_z) and RMS Radius (sig_r) of Beam in Aluminum as a Function of Energy ($E_0 = 12.5$ keV).

20 MeV electrons. For applications including radiation effects studies of electrical circuits, spatial dimensions in the tens of micrometers are important.

Figure 5 indicates that the Random Hinge method estimates $\sigma_z(E)$ to be about 6.3% higher than MCH and analog Monte Carlo for all energies. Although Random Hinge determines $\sigma_r(E)$ within 1.0% at lower energies, the values of the rms radius are about 4.1% too low at higher energies. Kawrakow and Bielajew (1998) have shown that indeed Random Hinge limits to the correct values of $\sigma_r(E)$ as $E \rightarrow 0$. Furthermore, they have also indicated that Random Hinge's estimates for $\sigma_z(E)$ do not improve with decreasing energies. As expected, MCH calculations agree with the analog results for all energies.

The depth-dose curve for the 12.5 keV beam is illustrated in Figure 6. The dose predicted by MCH resembles the analog Monte Carlo distribution more closely than the results predicted by Random Hinge. However, as stated before, preserving spatial moments does not guarantee that the dose estimates will be exact. Nevertheless, Figure 6 indicates that MCH's capability of preserving moments enhances the accuracy of dose calculations over methods which do not preserve higher-order moments. Because of fairly isotropic scattering, the number of electrons that backscatter is appreciable. The Random Hinge scheme, which conceptually models backscattering more effectively than Berger's methods, predicts the dose quite accurately for negative depths ($z < 0$).

6. Conclusions

In this paper we have described the three-dimensional MCH algorithm, which determines electron positions more accurately than current CH methods. By evaluating the zeroth-, first-, and second-order spatial moments of the Boltzmann equation (given $\underline{\Omega}$ and s), MCH preserves the mean position and the standard deviation in the mean position *exactly* for electrons of any energy that have traveled any number of

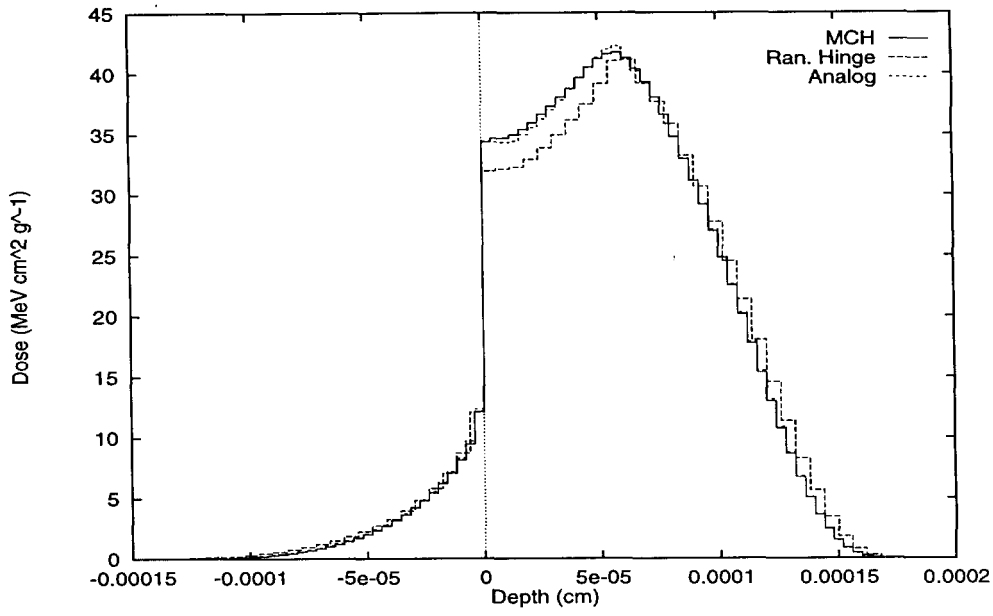

Figure 6: Dose Deposited as a Function of Depth into Aluminum ($E_0 = 12.5$ keV).

steps. This enables MCH to provide electron transport calculations more accurately than existing CH schemes. This is most evident when the scattering is more isotropic (problems involving low energy electrons or electron transport in high-Z materials). Here, the assumptions underlying conventional Condensed History are not closely met. Furthermore, we have shown that the MCH algorithm provides results that compare very well to the results from costly analog Monte Carlo.

Unfortunately, the MCH scheme is more costly per history than current methods. This is due to the time required to evaluate the spatial moment functions which, like the Goudsmit-Saunderson distribution, are defined by infinite series. In the future, we seek to improve the efficiency of MCH simulations by reducing this expense. Techniques such as Molière theory (1953) and Bielajew's improvement (1994) already exist for approximating the Goudsmit-Saunderson infinite series with simpler functions. Perhaps these methods could be extended to simplify the evaluation of the first- and second-order moments.

Another approximation involved with Condensed History is the assumption of an infinite medium. This approximation is inherent in both existing and our MCH algorithms. The spatial moments derived in Section 2 are based on an infinite medium and cannot be preserved exactly when electrons cross material interfaces. In other publications (Tolar, 1999 and 2001), we discuss various compromises that have been made to Condensed History algorithms when dealing with finite medium problems.

ACKNOWLEDGMENTS

This work was performed under the auspices of the U.S. Department of Energy by the University of California Lawrence Livermore National Laboratory under contract W-7405-Eng-48.

REFERENCES

Ballinger, C.T. et al., 1992. "Single-Scatter Monte Carlo Compared to Condensed History Results for Low Energy Electrons," *Nucl. Instrum. Methods Phys. Research,* **B72**, 19.

Baró, J., Sempau. J., Fernandex-Varia, J.M., and Salvat, F., 1995. "PENELOPE: An Algorithm for Monte Carlo Simulation of the of the Penetration and Energy Loss of Electrons and Positrons in Matter," *Nucl. Instrum. Methods Phys. Research,* **B100**, 31.

Berger, M.J., 1963. "Monte Carlo Calculation of the Penetration and Diffusion of Fast Charged Particles," *Methods in Computational Physics,* Vol. 1, Academic Press, New York, p. 135.

Bethe, H.A., 1953. "Molière's Theory of Multiple Scattering," *Phys. Rev.,* **89**, 1256.

Bielajew, A.F., 1994. "Plural and Multiple Small-Angle Scattering from a Screened Rutherford Cross Section," *Nucl. Instrum. Methods Phys. Research,* **B86**, 257.

Goudsmit, S. and Saunderson, J.L., 1940. "Multiple Scattering of Electrons," *Phys. Rev.,* **57**, 24.

Kawrakow, I. and Bielajew, A.F., 1998. "On the Condensed History Technique for Electron Transport," *Nucl. Instrum. Methods Phys. Research,* **B142**, 253.

Larsen, E.W., 1992. "A Theoretical Derivation of the Condensed History Algorithm," *Ann. Nucl. Energy,* **19**, 701.

Larsen, E.W., Miften, M.M., Fraass, B.A., and Bruinvis, I.A.D., 1997. "Electron Dose Calculations Using the Method of Moments," *Med. Phys.,* **24**, 111.

Lewis, H.W., 1950. "Multiple Scattering in an Infinite Medium," *Phys. Rev.,* **78**, 526.

Shultis, J.K. and Faw, R.E., 1996. *Radiation Shielding*, Prentice-Hall, Upper Saddle River, New Jersey, p. 386.

Tolar, D.R. Jr., 1999. "Advanced Multiple Scattering Algorithms for Electron Transport," *Ph.D. Dissertation*, University of Michigan.

Tolar, D.R. Jr. and Larsen, E.W., 2001. "A Transport Condensed History Algorithm for Electron Monte Carlo Simulations," *Nucl. Sci. Eng.,* to appear.